Nat. Hazards Earth Syst. Sci., 11, 3135–3149, 2011
www.nat-hazards-earth-syst-sci.net/11/3135/2011/
doi:10.5194/nhess-11-3135-2011
© Author(s) 2011. CC Attribution 3.0 License.

Natural Hazards and Earth System Sciences

Impact of ASAR soil moisture data on the MM5 precipitation forecast for the Tanaro flood event of April 2009

G. Panegrossi[1], **R. Ferretti**[1,2], **L. Pulvirenti**[3], **and N. Pierdicca**[3]

[1]CETEMPS, University of L'Aquila, Via Vetoio 19, Coppito, AQ, Italy
[2]Department of Physics, University of L'Aquila, Via Vetoio 19, Coppito, AQ, Italy
[3]Department of Information Engineering, Electronics and Telecommunications, Sapienza University of Rome, Via Eudossiana 18, 00184 Rome, Italy

Received: 14 April 2011 – Revised: 11 August 2011 – Accepted: 1 October 2011 – Published: 5 December 2011

Abstract. The representation of land-atmosphere interactions in weather forecast models has a strong impact on the Planetary Boundary Layer (PBL) and, in turn, on the forecast. Soil moisture is one of the key variables in land surface modelling, and an inadequate initial soil moisture field can introduce major biases in the surface heat and moisture fluxes and have a long-lasting effect on the model behaviour. Detecting the variability of soil characteristics at small scales is particularly important in mesoscale models because of the continued increase of their spatial resolution. In this paper, the high resolution soil moisture field derived from ENVISAT/ASAR observations is used to derive the soil moisture initial condition for the MM5 simulation of the Tanaro flood event of April 2009. The ASAR-derived soil moisture field shows significantly drier conditions compared to the ECMWF analysis. The impact of soil moisture on the forecast has been evaluated in terms of predicted precipitation and rain gauge data available for this event have been used as ground truth. The use of the drier, highly resolved soil moisture content (SMC) shows a significant impact on the precipitation forecast, particularly evident during the early phase of the event. The timing of the onset of the precipitation, as well as the intensity of rainfall and the location of rain/no rain areas, are better predicted. The overall accuracy of the forecast using ASAR SMC data is significantly increased during the first 30 h of simulation. The impact of initial SMC on the precipitation has been related to the change in the water vapour field in the PBL prior to the onset of the precipitation, due to surface evaporation. This study represents a first attempt to establish whether high resolution SAR-based SMC data might be useful for operational use, in anticipation of the launch of the Sentinel-1 satellite.

Correspondence to: G. Panegrossi
(giulia.panegrossi@gmail.com)

1 Introduction

It has been extensively shown that land surface processes play an important role not only in large-scale atmospheric models (Chen and Avissar, 1994a; Polcher et al., 1998), but also in mesoscale atmospheric processes, including precipitation (Avissar and Pielke, 1989; Chen and Avissar, 1994b; Chen et al., 2001; Xiu and Pleim, 2001). Surface moisture and heat fluxes influence the Planetary Boundary Layer (PBL) structure, which in turn influences precipitation through a variety of factors and processes that characterize land surface interaction with the atmosphere.

Soil evaporation is one key process affecting the PBL structure. Its effect is determined not only by the soil conditions (the degree of shading of the crop canopy and the amount of water available at the evaporating surface), but also by a number of climatological parameters: solar radiation, air temperature, air humidity, and wind speed. Depending on the atmospheric conditions, a significant variation of land surface moisture can produce an increase, decrease or no change of cloud amount and precipitation. Differences in the thermodynamic structure of the atmosphere result in different responses of the atmosphere to land surface moisture, depending on the role of synoptic forcing. Moreover, the high spatial variability of soil moisture conditions can generate strong air temperature gradients, differences in the partitioning between surface sensible heat, and latent heat fluxes, favouring or inhibiting local turbulence (Chen and Avissar, 1994b).

The representation of the interactions between land and atmosphere, the accuracy of the land surface model used and the representativeness of the parameters used to describe the surface conditions have a strong impact on the PBL and in turn, on the cumulus and cloud schemes and on the weather forecast. Mesoscale models include advanced and robust land surface models (LSMs) in order to properly represent

the ground and subsequently capture the mesoscale structures in the free atmosphere and the PBL forced by the ground surface. However, LSMs require a large number of parameters related to the vegetation and soil state; unfortunately it is difficult to obtain measurements of these parameters at high resolution on extended areas. A major problem is related to the initialization of soil moisture and temperature fields in the mesoscale models, because soil moisture is a very important component in the land surface modelling system. Even in a "perfect LSM," inadequate initial soil moisture fields can introduce major biases in the partitioning of surface energy and have a long-lasting effect on the model's behaviour (Chen and Dudhia, 2001). Pleim and Gilliam (2009) pointed out that if land surface models are applied in weather forecast, such as the fifth generation Pennsylvania State University–National Center for Atmospheric Research Mesoscale Model (MM5) and Weather Research and Forecasting Model (WRF), they perform well only if some source of realistic initialization for soil moisture is provided. Operational systems often use a Land Data Assimilation System (LDAS), which is essentially an offline version of the LSM forced with observed precipitation, radiation, and analyzed meteorology, so that the forecast starts with optimal soil moisture fields (e.g. Mitchell et al., 2004; Chen et al., 2007; Alapaty et al., 2008). Another way to initialize soil moisture is through dynamic adjustment within the mesoscale model simulation where soil moisture is nudged according to differences between modelled and analyzed observations of 2-m temperature and relative humidity, as described by Pleim and Xiu (2003). Soil moisture, particularly root zone soil moisture, is a strong factor controlling surface evaporation and evapotranspiration and thereby, the partitioning of available surface energy into latent and sensible heat flux.

Chen and Avissar (1994a) pointed out that the land surface heterogeneity (vegetation, moisture and topography) has a strong impact on shallow clouds and precipitation. Convergence is formed near the boundary between wet and dry regions and updrafts develop at the circulation front. Rabin et al. (1990) have shown that the spatial variability of land surface moisture has a strong impact on cumulus clouds. Detecting the variability of soil characteristics at small scales is particularly important in mesoscale models because of the continue increase of their spatial resolution. Indeed, sensitivity to spatial gradients of soil moisture has been proved by past studies with mesoscale atmospheric models (Dubois et al., 1995).

Spaceborne microwave remote sensing sensors have the potential for extracting spatial soil moisture information because of the dependence of microwave backscattering over bare or scarcely vegetated terrains on the dielectric constant of soils, which is in turn influenced by the volumetric moisture content. Low resolution (25 km) soil moisture content (SMC) data derived from the measurements of the advanced scatterometer (ASCAT) on board METOP are presently assimilated in the European Centre for Medium-Range Weather Forecast (ECMWF) numerical weather prediction (NWP) model. However, the only instruments that can fulfil the spatial resolution requirements needed for detecting small scale SMC variations are Synthetic Aperture Radar (SAR) systems (Verhoest et al., 2008).

SAR observations cover large areas with a regular periodicity, but the long revisit time of the currently available SAR sensors operating at L- and C-bands is a critical issue for weather forecasting applications, while X-band radars such as those mounted aboard COSMO-SkyMed (Constellation of small Satellites for Mediterranean basin Observation) are not particularly suitable for SMC estimation because of the short penetration depth of X-band radiation and its sensitivity to soil roughness. However, the temporal resolution of SAR data will be considerably improved by the future generation of SAR systems such as Sentinel-1, working at C-band, envisaged to launch in 2013.

Once Sentinel-1 observations are available, they are expected to be very useful in improving the performances of both hydrological and NWP models through a spatially accurate determination of soil conditions. Moreover, the SMC values retrieved by SAR can be compared to those predicted by the NWP models to validate and calibrate the latter. However, it is essential to establish whether these expectations will be met. In particular, it is very important to explore if there are specific meteorological conditions and characteristics of the NWP model that would make the forecast more or less influenced by high resolution moisture field as initial conditions.

In this study, SMC retrievals from the C-band Advanced Synthetic Aperture Radar (ASAR) on board ENVISAT, which basically represents the precursor of Sentinel-1, are used to initialize the soil moisture field in MM5. The goal is the evaluation of the impact of using soil moisture estimates from SAR as initial condition in the MM5 on the precipitation forecast. The case selected for this study is a flood event that occurred on 26–28 April 2009 in the Tanaro river basin in the Piedmont region in Northern Italy. This event represents an optimal case study for our investigation. On one hand, floods occurring in small sized river catchments, such as the Tanaro basin, represent the most destructive natural hazards in the Mediterranean region (Tramblay et al., 2010), so that extensive efforts are worthwhile to accurately forecast them. On the other hand, the Tanaro basin includes a large variety of land cover classes (also urban areas and forests in which retrieving SMC is unfeasible), so that moisture estimates from low resolution data are not particularly suitable for this case study. Fortunately, ASAR observed the Tanaro basin on 24 April in Image Swath 2 (IS2) mode (30 m of range resolution) and the corresponding backscattering data have been used to produce a soil moisture map.

The purpose of this study is to answer to the following questions:

- How do SAR-derived SMC data compare with the SMC field in the NWP analysis generally used to initialize MM5?
- How sensitive are MM5 precipitation forecast and PBL water vapour field to high resolution initial soil moisture data?
- Are there some constraints to the model set-up to make the forecast sensitive to the soil moisture?
- Could the use of future Sentinel-1 SMC data be useful for forecasting purposes and would it be worth using these data operationally?

This paper is organized as follows. Section 2 gives a brief description of the meteorological conditions that led to the Tanaro flood event. In Sect. 3, the ASAR retrieval algorithm will be briefly described as well as the MM5 set-up used in this study, with particular emphasis on the Land Surface Model. Finally, the procedure used to initialize MM5 with ASAR retrieved SMC data will be discussed. Section 4 will present the results of the MM5 simulations, and the comparison of the results with in situ precipitation measurements. In Sect. 5, the conclusions from this study are drawn and a discussion about future work and applications is presented.

2 Case study: the Tanaro flood event of April 2009

The SAR data used in this paper concern the overflowing of the Tanaro River, close to the city of Alessandria (Northern Italy), which occurred on 26–28 April 2009. Fortunately, it did not cause either damage to buildings, or casualties. However, many crops were destroyed and approximately 6000 people were evacuated (Pulvirenti et al., 2011). Such an event was caused by widespread rainfall starting on 26 April 2009; between 26 and 28 April, 150–200 mm of rain fell on the Tanaro basin. Precipitation ended on 29 April. It is worth noting that the study area was historically subject to flooding, such as that which happened in 1994 causing 70 casualties and over 2000 homeless (Pierdicca et al., 2008a).

The event was characterized by a strong synoptic scale forcing and orographic lifting. Similarly to the Piedmont floods of 1994 (Ferretti et al., 2000) and 2000, an upper level trough positively tilted entered the Mediterranean region from the Northwest, and was associated with a low-level depression. At 00:00 UTC, 26 April 2009, the trough axis ran from Gibraltar to London leading to a south-westerly flow of humid air in the upper levels (not shown), which was associated with a low level easterly wind advecting air dryer than at upper levels (Fig. 1). Both the humidity gradient and the vertical wind shear allowed for moderate widespread precipitation during the day, intensifying correspondingly in the northern and southern parts of the Piedmont regions due to orographic lifting. In the following 36 h, the trough deepened in the Mediterranean and its axis rotated counter-clockwise, leading to a surface low centered in the Northern Tyrrhenian Sea. This led to an intensification of both the south-south-easterly winds at upper and low levels in the eastern Tyrrhenian sea and the easterly winds in the Pò Valley, intensifying the low level flow convergence in the Tanaro basin (Fig. 1c and d). This meteorological condition led to intense and widespread precipitation during 27 April, with the most intense precipitation in the pre-Alpine and Alpine region in Piedmont and in the South of Liguria and a line of convective precipitation in the valley. The spatial distribution of the most intense precipitation has been determined mainly by the interaction of the large-scale forcing with the topography: the L-shaped structure of the Alps as well as the humidity gradient and the wind speed, both concurring to develop a line of convergence, have been already proposed as the main factors leading to heavy events in the Piedmont region (Rotunno and Ferretti, 2001). On 28 April, the system moved towards the Northeast, and a new Atlantic perturbation entered the region producing an attenuation of the precipitation in the South but intense precipitation in the Alpine regions.

Rain gauge data for this event have been used as ground truth. They have been made available by the Italian Department of Civil Protection within the framework of a study funded by the Italian Space Agency (ASI) named PROSA (Italian acronym for Satellite Observation Products for Meteorological Alerts), which was conceived as a pre-operational system whose main purpose is the evaluation of the utility of satellite remote sensing products in case of weather alert. Within this project, consisting of many different tools such as remote sensing data processors and numerical weather prediction models, the hourly precipitation data from the Italian network of rain gauge stations have been collected for the whole year 2009. The rain gauge data available for the Tanaro event were used to assess the model's ability to predict the amount and the spatial distribution of the observed precipitation field, and to evaluate the effect of using ASAR retrieved SMC on MM5 forecast. A rain gauge data quality control has been performed to check for any sort of failure of the rain gauges. The data available at 186 stations within MM5 domain 4 (see Sect. 3.2 and Fig. 3) have been selected for the days of interest in this study. In order to be able to compare the measured rainfall with the MM5 results, the rain gauge data have been interpolated and remapped at the MM5 grid points. Figure 2 (left panel) shows the spatial distribution of the rain gauge in domain 4 and the rainfall map (hourly precipitation in $\mathrm{mm\,h^{-1}}$) resulting from the 2-D interpolation on the MM5 grid points. The data in these figures refer to 27 April, 12:00 UTC, when the registered precipitation was highly variable over the domains and quite intense in some areas. Unfortunately, domain 4 coincides with a region were rain gauge stations are quite sparse. On the other hand, Fig. 2 (right panel) shows the rain gauges' distribution in MM5 domain 3 (see Sect. 3.2 and Fig. 3), where 643 rain stations are selected as a result of the quality control procedure.

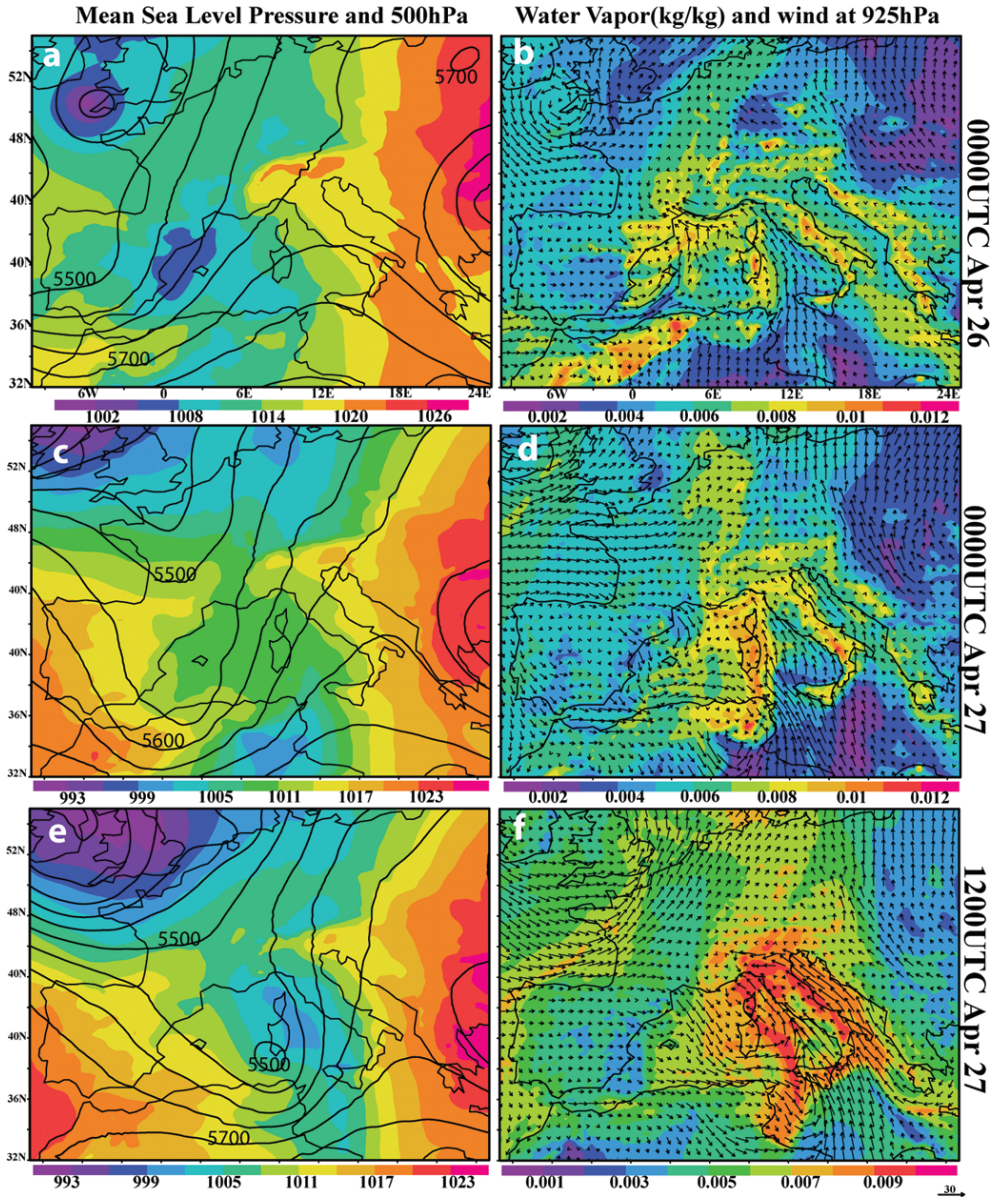

Fig. 1. ECMWF analyses mean sea level pressure (shaded) and 500 hPa geopotential height (contour interval = 50 gpm) on the left side; 925 hPa water vapour mixing ratio (kg kg^{-1}) and wind on the right side. For 26 April 2009 at 00:00 UTC on the top panel, 27 April 2009 at 00:00 UTC on the middle panel, 27 April 2009 at 12:00 UTC in the bottom panel.

The sparse distribution of the rain gauges in domain 4 adds uncertainty to the results of the 2-D interpolation and to the rainfall at the MM5 grid points. The use of radar as ground truth has been also evaluated by analyzing the available radar rainrate estimates available for the event, but the comparison with rain gauges, has shown that the radar was not always able to detect high intensity rain in the mountains. Therefore, in spite of the limitations of the rain gauge network previously discussed, rain gauge data will be used for the comparison with the model output and the discussion in the following sections.

3 Methodology

The results of NWP forecast are dramatically affected by the numerous assumptions, approximations, and parameterizations used in the model. Moreover, the remote sensing retrieval of soil moisture is made difficult by the presence of vegetation, type of soil, and the atmospheric conditions that characterized the environment at the time of the observation. In order to better understand the results of this study, it is worth describing the main features of these limitations, and relate the results to the assumptions in the algorithm to retrieve SMC from SAR data or in the MM5

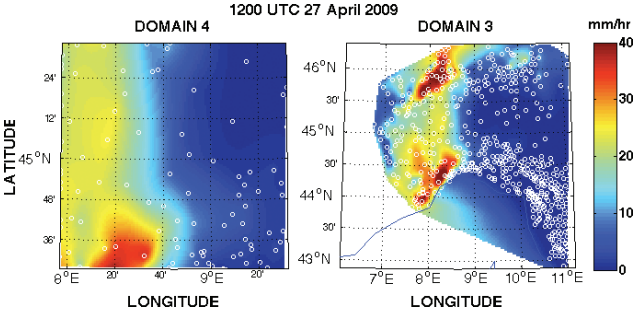

Fig. 2. Rain gauge coverage (white circles) and measured precipitation rate (in mm h^{-1}) at 12:00 UTC, 27 April, interpolated on MM5 grid points of domain 4 (left panel) and domain 3 (right panel).

parameterizations. In this section, the SMC retrieval algorithm from ENVISAT/ASAR measurements, the MM5 configuration used for this study, and the procedure used to initialize MM5 with ASAR SMC data are described.

3.1 SMC retrieval algorithm

SMC estimation from SAR microwave data was widely investigated in the past, because SAR measurements are characterized by high spatial resolution (30 m for ASAR), considerably better than that achievable by microwave radiometers and scatterometers, and they can be collected in almost any meteorological condition and both during day-time and night-time (Pierdicca et al., 2010). Basically, the capability of microwave remote sensing sensors to retrieve soil moisture depends on the large difference between the dielectric constant (ε) of dry soil ($\sim$3–6) and of water that, below its relaxation frequency ($\sim$20 GHz), is approximately in the order of the ε in static conditions (when frequency goes to zero the real part of the relative permittivity of water is equal to about 78.3). Since when radiation impinges on the terrain, the intensity of scattering is related to the value of the soil dielectric constant, it is possible to estimate soil moisture by measuring the amount of radiation that is scattered back towards the radar antenna, i.e. the backscattering coefficient σ^0. Actually, not only the dielectric, but also the geometric (i.e. roughness) properties of the terrain contribute to σ^0. Considering also the large amount of unknown effects on the radar measurements, SMC retrieval from microwave radar data is still a challenging problem, especially if the data of a single-parameter (i.e. single frequency, observation angle and polarization) SAR are used.

To mitigate the effects of the nuisance parameters, i.e. those that, besides soil moisture, influence the backscattering, an appropriate radar configuration must be chosen (e.g. observation at low incidence angle to reduce the effect of soil roughness and of the possible presence of vegetation), and a priori information on these parameters should be introduced in the retrieval algorithm. Moreover, ancillary data providing information on land cover and on the presence and the state of vegetation have to be also considered (Pierdicca et al., 2009).

The algorithm designed to retrieve soil moisture is focused on the Bayesian theory of parameter estimation. The Maximum A Posteriori (MAP) probability criterion is used to retrieve the soil moisture by inverting a forward scattering model as described in Pierdicca et al. (2008b). Indeed, MAP is numerically implemented by means of a Monte Carlo method that requires the statistical generation of a database of soil parameters matched with radar measurements. The latter are generated by the forward backscattering model proposed by Oh et al. (2002). The algorithm uses land cover maps (e.g. CORINE) to flag areas in which soil moisture cannot be estimated (e.g. urban areas, forests, water bodies), as well as optical data to compute the Normalized Difference Vegetation Index (NDVI) providing information on the state of vegetation. The effect of sparse vegetation on the radar backscattering is accounted for through the semi-empirical model proposed by Attema and Ulaby (1978).

The soil moisture mapping procedure has been calibrated and validated within the PROSA project. For the calibration/validation activity, in situ ground truth data of soil moisture and roughness were collected during a period of seven years in the Tanaro basin. Gathering real roughness data has allowed us to establish a reliable range of roughness values to be used as a priori information in the retrieval algorithm. It is worth noting that the experimental ground campaigns were accomplished simultaneously with the SAR acquisitions over the test basin.

3.2 MM5 set-up

The MM5V3 model from NCAR is used for this study; this is a non-hydroststic, fully compressible model using a terrain following vertical coordinate (Dudhia, 1993; Grell et al., 1994). The simulations are performed using 4 two-way nested domains respectively at 27 km, 9 km, 3 km, and 1 km horizontal resolution, as shown in Fig. 3. The inner domain has 120×120 grid points, and it fully includes the area covered by ENVISAT/ASAR. The model configuration is characterized by 33 vertical sigma levels from the surface up to 100 hPa.

The MM5 physical parameterizations used for the experiments are:

- the Gayno-Seaman for the planetary boundary layer (PBL). This scheme is particularly feasible for humid areas because of using liquid water potential temperature as a conserved variable, allowing the PBL to operate more accurately in saturated conditions (Ballard et al., 1991; Shafran et al., 2000);
- the Kain-Fritsch 2 (KF2) cumulus convection parameterization is applied to domains 1 and 2 (Kain, 2002), whereas no cumulus scheme is used for domains 3 and 4;

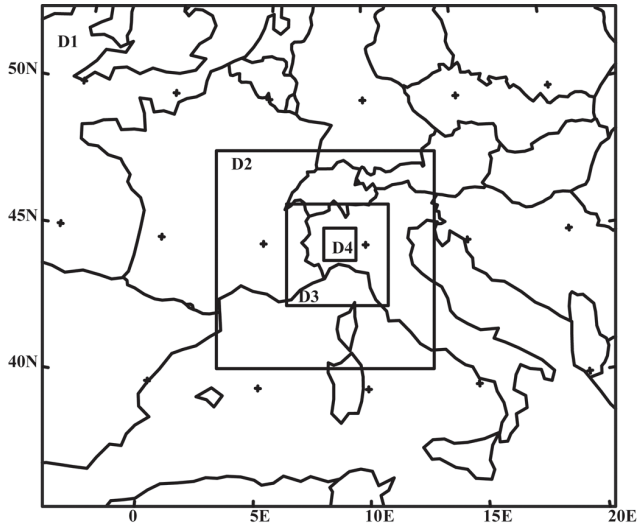

Fig. 3. Four two-way nested domains of the MM5 model at 27 km, 9 km, 3 km, and 1 km horizontal resolution.

- the Reisner 2 scheme is used for microphysics (including mixed-phase hydrometeors and graupel) (Reisner et al., 1998; Thompson et al., 2004);
- the NOAH scheme is used as Land Surface Model (LSM) (Chen and Dudhia, 2001).

In order to understand the potential impact of soil moisture on the MM5 precipitation forecast, it is worth describing some of the main aspects of the NOAH LSM. It is a stand-alone, 1-D column model which can be executed in either coupled or uncoupled mode. The model applies finite-difference spatial discretization methods and a Crank-Nicholson time-integration scheme to numerically integrate the governing equations of the physical processes of the soil-vegetation-snowpack medium. The input variables required are annual mean surface temperature, seasonal vegetation fractions, as well as initial soil moisture and temperature at different layers. The coupling of the NOAH LSM and the PBL occurs at the surface layer through the exchange of the surface latent and sensible heat fluxes, water flux terms of the surface water balance, and the air temperature, humidity, and wind conditions. The NOAH land-surface model predicts soil moisture and temperature in each of the four layers, canopy moisture, and water-equivalent snow depth. It also calculates surface and underground runoff; it includes effects like soil conductivity and gravitational flux of moisture and it uses vegetation and soil types in handling evapo-transpiration and direct soil evaporation. The change in soil moisture is governed by Richard's equation for soil water movement (Chen and Dudhia, 2001), where the source/sink term is given by the positive/negative balance of three main processes: precipitation, runoff, and evaporation (the infiltration results from the difference between precipitation and runoff). If the infiltration exceeds the evaporation, the source/sink term gives a positive contribution to the Richard's equation, while the contribution is negative if the evaporation exceeds the infiltration.

The evaporation processes are a function of soil moisture, vegetation type, rooting depth/density, and vegetation cover. The total evaporation E is:

$$E = E_{\mathrm{dir}} + E_{\mathrm{t}} + E_{\mathrm{c}} + E_{\mathrm{snow}} \quad (1)$$

where E_{dir} is the direct evaporation, the E_{t} is the transpiration through plant canopy, E_{c} is the evaporation from canopy intercepted rainfall, and E_{snow} is the sublimation from snowpack. The terms where soil moisture comes into play are E_{t} and E_{dir}. E_{t} represents the evaporation of water from plant canopy via uptake of the roots in the soil, which is determined not only by the green vegetation fraction, but also by the type of vegetation, the amount of solar radiation, the air temperature, air humidity, and the soil moisture (through the canopy resistance term). E_{dir} is the main mechanism directly influenced by the soil moisture, responsible for the direct release of soil moisture in the PBL, through the exchange between the skin layer and the first MM5 vertical level, and it is parameterized as follows:

$$E_{\mathrm{dir}} = (1 - \sigma_{\mathrm{f}})\beta E_{\mathrm{p}} \quad (2)$$

where σ_{f} is the green vegetation fraction (5 yr NDVI climatology of monthly values), E_{p} is the potential evaporation (the amount of evaporation that would occur if a sufficient water source were available), and β is the normalized water content, defined as:

$$\beta = (\theta - \theta_{\mathrm{wp}})/(\theta_{\mathrm{cap}} - \theta_{\mathrm{wp}}) \quad (3)$$

where θ is the volumetric soil moisture content (fraction of unit soil volume occupied by water), θ_{wp} is the wilting point (critical soil moisture at (or below) which evaporation ceases), and θ_{cap} is the field capacity (maximum allowed soil moisture). If soil moisture exceeds the field capacity, β is set to 1, and the direct evaporation equals the potential evaporation. The values of θ_{wp} and θ_{cap}, as well as other soil dependent parameters, are given in a look-up table with 19 soil categories. The US Geological Survey (USGS) landuse look-up table with 27 categories including urban/built up land gives all the vegetation parameters necessary for the canopy evaporation processes. The soil and vegetation characterization for the MM5 domains of the Tanaro simulation are given by the USGS database, affected by a low horizontal resolution (30 arc sec, approximately 1 km) so that does not adequately represent the soil and vegetation variability as it should to be consistent with the high resolution (30 m) ASAR SMC retrieved field.

The change in the soil moisture initial condition directly impacts E_{dir} and, indirectly E_{t}, through the canopy resistance dependence on soil moisture. The change of initial soil moisture impacts E_{dir} only when its value varies between θ_{wp} and

θ_{cap} (Eqs. 2 and 3). In the presence of moderate to heavy precipitation, when the infiltration term is positive and exceeds the evaporation, θ approaches θ_{cap}. In this case, the direct evaporation process is governed by E_p, (times the vegetation fraction σ_f) and it becomes independent of the initial soil moisture conditions. Therefore, it is reasonable to think that the initial soil moisture conditions determine the amount of evaporation before the onset of precipitation, and that the SMC variability and content might influence the time, the location, and the amount of the initial precipitation.

The ECMWF analysis at 0.25° for temperature, wind speed, relative humidity, and geopotential height are interpolated to the MM5 horizontal grid and to sigma levels to produce the model initial and boundary conditions. The model simulations started at 00:00 UTC, 25 April and lasted 48 h. Two simulations were carried out, using the same model set-up, and the same initial and boundary conditions (from ECMWF analysis), except for the initial soil moisture field. The first simulation was performed using ECMWF analysis for the initial soil moisture field from now on ($MM5_E$), and the second one using ASAR SMC data ($MM5_S$).

3.3 MM5 initialization with ASAR SMC data

The ASAR image used to produce a soil moisture map was acquired on 24 April 2009, at 20:53 UTC in ascending orbit, 23° of observation angle, in vertical polarization. Due to the long revisit time of the ENVISAT platform (i.e. 35 days), no other ASAR images are available for this event. The soil layer depth corresponding to the ASAR SMC retrieved data is of the order of a few centimetres (1–5 cm). In the framework of the validation activity of the PROSA project, in situ ground truth data of soil moisture were collected on 24 April 2009, so that we have been able to compare the retrievals with actual data obtaining good results (root mean square error less than 4 %). Therefore, we can trust the reliability of the generated SMC map. The results of the ASAR SMC retrieval, interpolated to the MM5 inner domain grid points, is shown in Fig. 5. It has to be noted that, to use these data to initialize MM5, their horizontal resolution has to be comparable to that of MM5. Therefore, the soil moisture data have to be degraded: they are initially produced at a resolution of 30 m (ASAR data) and have been averaged and interpolated to MM5 inner domain grid points that is 1 km.

The purpose of this study is to investigate the impact of initial soil moisture conditions on the timing and the location of the onset of precipitation and on the evolution of the precipitation forecast. Since there was no precipitation between 24 and 25 April, the simulations start on 25 April, at 00:00 UTC, to be able to capture the early phase of the event on 26 April, and to follow its evolution until 27 April, 00:00 UTC; this choice allows for staying within the first 48 h of simulation, when the MM5 forecast is more reliable, while does not allow for capturing the event during its most intense phase characterized by the presence of convective precipitation. In

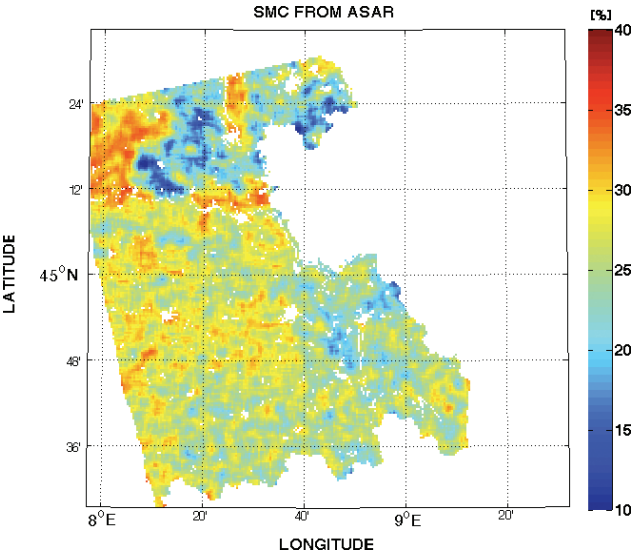

Fig. 4. Top layer SMC (%) retrieved from ASAR on 24 April, 20:53 UTC and interpolated to MM5 inner domain grid points. White areas are those not observed by ASAR or not included in the Tanaro basin or flagged because the soil was not bare or scarcely vegetated.

order to have initial soil moisture conditions more consistent with those at the time of the ASAR overpass so that the use of ASAR soil moisture measurements is reasonable, we impose the simulation to start at night time. This also allows for MM5 to have the right spin-up time (approximately six hours) during hours with little or no soil direct evaporation (from 00:00 UTC until 06:00 UTC). At the end of the model spin-up, the incoming solar radiation will enhance the soil and canopy evaporation processes (depending on other factors such as the degree of synoptic forcing, local thermodynamic conditions, wind speed, and air humidity), making it possible to evaluate their effects on the PBL water vapour field and heat fluxes throughout their full evolution. To study the impact of the SMC on the forecast during the most intense phase of the event (27 April 2009), a model simulation starting on 26 April, 00:00 UTC would be necessary. This would imply initializing the soil moisture with measurements performed 48 h in advance, which is quite questionable. An attempt was made in this sense (model results of this simulation are not shown), but, because of the closeness of the start time to the precipitation onset, and because of the lack of evaporation during the night, there was little impact of using the ASAR SMC on the forecast. In fact, by the time the evaporation starts, the soil is saturated and the SMC initial conditions have no longer an effect on the forecast.

The $MM5_E$ simulation is initialized using the ECMWF soil moisture data available at four soil layers, whose depth ranges between 0–7 cm (layer 1), 7–28 cm, (layer 2), 28–100 cm (layer 3), and 100–200 cm (layer 4). The ECMWF soil moisture field is the result of the current operational soil

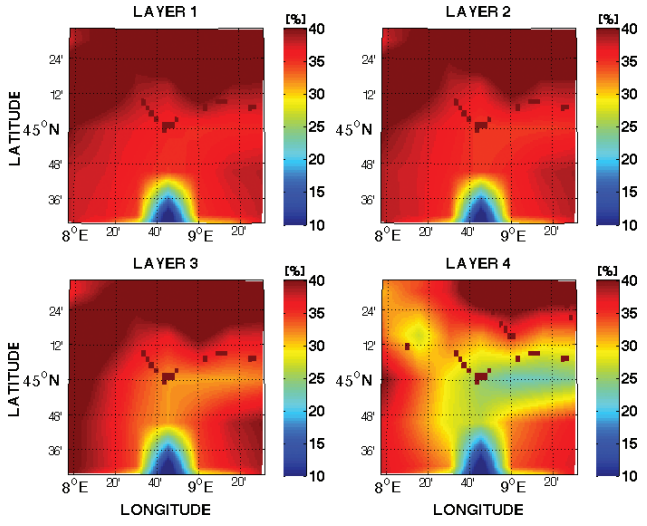

Fig. 5. Volumetric SMC (%) from ECMWF analysis at the four soil layers, on 25 April 2009, 00:00 UTC.

moisture analysis of the Integrated Forecasting System (IFS) at ECMWF, at $25 \times 25\,km^2$ horizontal resolution, where the ASCAT/METOP soil moisture is not incorporated. It is based on an Optimal Interpolation (OI) scheme using proxy observations (SYNOP) of 2-m air temperature and humidity (Mahfouf et al., 2000) (in IFS no soil moisture satellite data are used at this time). The OI soil moisture analysis relies on the link between soil variables and the lowest atmospheric level, and is subject to all the limitation of the IFS itself. The second run ($MM5_S$) is initialized using the soil moisture content retrieved by ASAR.

Figure 4 shows the SMC at the four LSM soil layers from ECMWF analysis in domain 4 (the inner domain). Large differences between the ECMWF SMC field and the ASAR SMC field are obtained by comparing Fig. 4 with Fig. 5 (top-left panel). The very wet soil moisture in ECMWF (Fig. 5, top-left panel) might be due to a IFS model positive precipitation bias, as reported by Chen and Dudhia (2001). Moreover, the ECMWF SMC shows some inconsistencies such as the very steep gradient and low soil moisture values in the southern portion of the domain. Unfortunately, no SAR observations are available for that portion of the domain. Moreover, the retrieval has not been feasible in densely vegetated areas, forests, urban areas and permanent water bodies. Nevertheless, in the portion of the domain where the SMC retrieval is available, the potential of ASAR to capture the high spatial variability of soil moisture is evident. For example, the sharp soil moisture gradient in the northwestern portion of the domain is due to the presence of rice fields, whose moisture is generally very high. Note that this high resolution feature is detectable only using SAR. A positive bias between the ECMWF SMC analysis and the observations can be assumed, the difference in the mean values being as high as 11.4 %. In order to take full advantage of the highly resolved ASAR SMC field and to take into account the bias found between the measurements and the ECMWF analysis, a procedure has been implemented to obtain a SMC field consistent with the observations to be used as initial condition for soil moisture in the MM5 simulation. This was achieved by merging the available retrieved SMC with the ECMWF SMC field in the inner domain, by correcting the biased ECMWF SMC in the outer domains, and by inferring the SMC values at all four soil layers.

The used methodology is summarized as follows:

1. at each MM5 grid point of the inner domain, the best fit polynomial to ECMWF SMC at the four soil layers is found;
2. ASAR SMC is averaged and interpolated to MM5 inner domain grid points and used as SMC at top layer, at the areas with valid ASAR data;
3. bias between the average ASAR SMC data (calculated over the grid points with valid ASAR data) and the average ECMWF SMC at top layer is found;
4. ECMWF data are corrected by the bias and used at grid points where ASAR data are not available, and a combined SMC field is built at the top layer;
5. the SMC value at the top layer and the best fit polynomial at each grid point are used to derive the SMC values at the three lower layers in the inner domain, building the corrected SMC field;
6. the bias found in the inner domain is used to correct ECMWF data also for the outer nested domains (domain 1, 2 and 3) in order to obtain an SMC field in all domains consistent with ASAR SMC data.

Figure 6 shows the result of the merging procedure in domain 4 between the ASAR retrieved SMC on 24 April 2009, at 20:53 UTC, and the ECMWF SMC on 25 April, 00:00 UTC (MM5 simulation start time) at all four model layers.

The SMC at the lower layers (layer 2 to layer 4) shows the high spatial variability in the areas where ASAR top layer SMC is available, but it also reflects the variability with depth of the ECMWF analysis data shown in Fig. 5. The SMC in each layer is scaled down to lower values consistently with the bias found between ECMWF analysis and SMC ASAR measurements.

4 Results and discussion

Both $MM5_E$ and $MM5_S$ are able to reproduce the major synoptic features of the event, described in Sect. 2, with the upper level trough positively tilted, the upper level humid air flow into the Tanaro basin, and the precipitation pattern

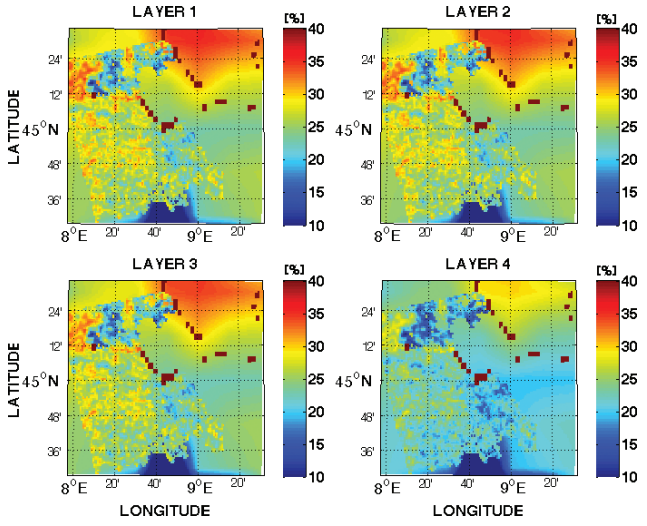

Fig. 6. Volumetric SMC (%) resulting from the merging procedure of the ASAR retrieval and the ECMWF analysis at the four MM5 soil layers, valid on 25 April, 00:00 UTC.

forced by orographic lifting. As both simulations progress, the model results clearly depict (not shown) the orographic origin of the most intense precipitation, evident from the highest amounts of accumulated precipitation in the mountainous regions in Liguria and in the pre-Alpine regions. However, major differences in the timing, the spatial distribution, and the amount of the precipitation are found between the two simulations, particularly in the high resolution domain. Since the interest of this paper is to assess the impact of using the high resolution ASAR SMC field on the precipitation forecast, this section focuses on the results for domain 4 only, showing the comparison between the two models' precipitation and between the model results and the rain gauge data available for the Tanaro flood event.

4.1 Qualitative comparison with rain gauge data

Figure 7 shows the 6 h accumulated precipitation in domain 4, the top panel from rain gauges, the middle panel for $MM5_E$ and the bottom panel for $MM5_S$. Left panels (i.e. the panels in first column) show the results at 03:00 UTC, 26 April, that is 27 h after the model start time, but at the rainfall onset. The rain gauges recorded a small amount of precipitation only on the western side of the domain. The $MM5_E$ shows both a larger amount of precipitation and more spread over the domain than $MM5_S$, which shows a precipitation pattern more similar to the observations. The model larger amount of accumulated precipitation is also due to an earlier onset of the precipitation with respect to the observed one. In $MM5_E$ significant amounts of precipitation is already found at 22:00 UTC, 25 April (with 70 % of the domain showing the presence of rain) whereas for $MM5_S$ it becomes significant at 01:00 UTC (with 40 % of the domain showing the presence of rain). The $MM5_S$ simulation is more consistent with the rain gauges in domain 4, which start recording precipitation around 03:00 UTC. The use of the ASAR-derived SMC, has a significant impact on both the quantity and the spatial distribution of the precipitation.

The panels in the second column of Fig. 7 concern 06:00 UTC. It can be noted that $MM5_E$ produces the presence of rain bands in the center of the domain which are not observed by rain gauges and generally overestimates the intensity of the precipitation. The use of the ASAR-derived SMC ($MM5_S$) tends to reduce this tendency, that is to reduce both the overestimation of the precipitation and the rainbands' structure. The third and fourth columns of Fig. 7 show the results at 08:00 UTC and 12:00 UTC, respectively. It can be observed that the large discrepancies in the rain field observed at the initial phase of the precipitation become less evident as the event progresses. The large scale features of the event become dominant over the small scale effects induced by the different initial SMC field, and the rain patterns in $MM5_E$ and $MM5_S$ become more similar as the simulations progress. Moreover, once the precipitation spreads over the domain in both simulations, the soil approaches saturated moisture conditions (i.e. the SMC approaches the field capacity, as explained in Sect. 3.2). Thus, there are the same soil conditions in both simulations. The differences in the rain pattern and in the intensity throughout the integration time are a consequence of the different initial SMC field, but these differences are more evident before soil saturation conditions are reached.

Similar conclusions can be drawn analyzing the 6 h accumulated precipitation on domain 3. Figure 8 shows the 6 h accumulated precipitation on domain 3 at 00:00 UTC (left panel) and 12:00 UTC (right panel) on 26 April. Both simulations overestimate the precipitation, especially on the windward side of mountains, a well known problem for MM5 as reported by many authors (i.e. Ferretti et al., 2003; Rotunno and Ferretti, 2003; Comellas et al., 2011). However, $MM5_S$ shows both rainfall amount and distribution closer to those observed. The left panel, regarding the event at its early stage, shows that the use of ASAR SMC allows better reproducing the areas of rain and no rain during the early phases of the event. The right panel shows that as the simulation progresses, the synoptic forcing and the orographic lifting cause heavier precipitation in the mountainous regions (in the North and in the South of the domain) in both simulations. Some differences in the precipitation amounts and locations between the two simulations are still found. These differences can be attributed only to the different local atmospheric conditions deriving from the soil moisture effect on the PBL during the early phase of the event.

In summary, the drier soil conditions measured by ASAR with respect to the ECMWF analysis have the effect of lowering the intensity of the rainfall at its early stages, delaying the onset of the precipitation and better locating the areas of precipitation. As the integration time progresses and the

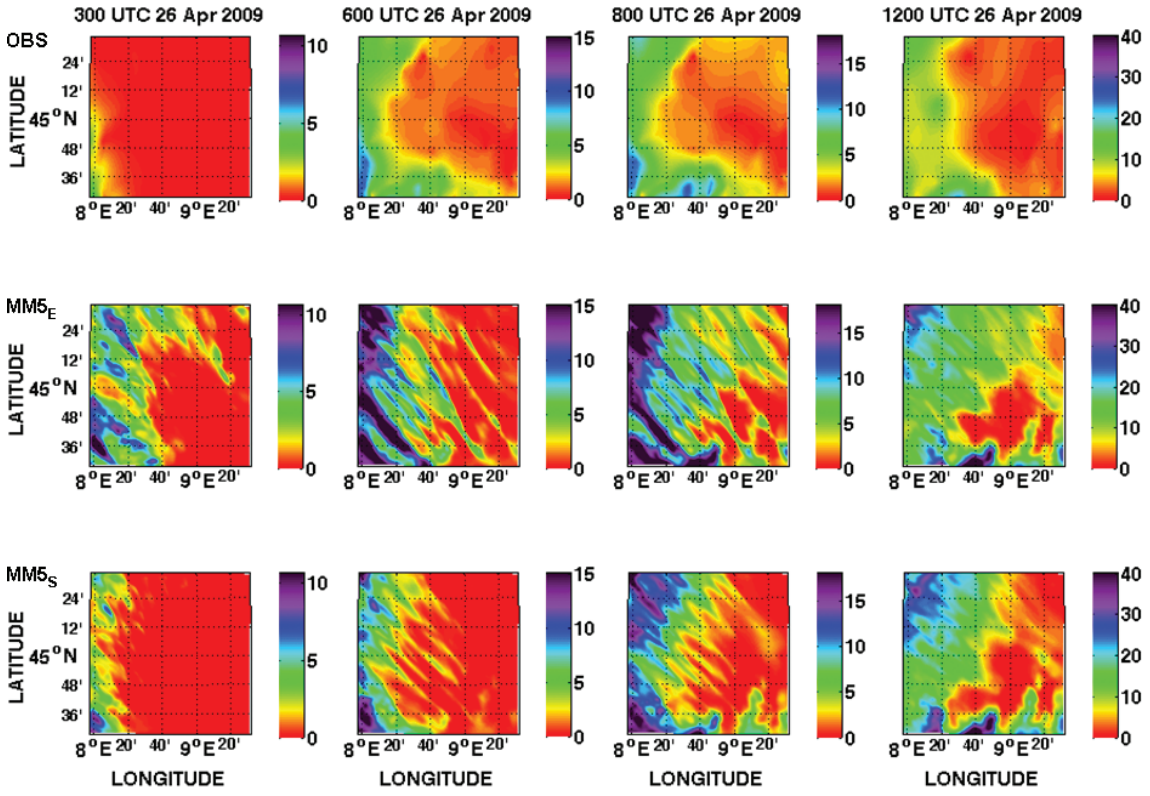

Fig. 7. 6 h accumulated precipitation (mm) on 26 April in domain 4 from rain gauges (top panels), $MM5_E$ run (middle panels), and $MM5_S$ run (bottom panels). First column: 03:00 UTC; second column: 06:00 UTC; third column: 08:00 UTC; fourth column: 12:00 UTC.

precipitation becomes more intense and spreads over the domain, $MM5_E$ still shows overall heavier precipitation than $MM5_S$, which shows a rain pattern more similar to that observed. These results imply that the effect of the soil evaporation process on the surface water vapour flux and on the partitioning between latent and sensible heat fluxes is driven mainly by the soil moisture conditions when the initial atmospheric conditions are unchanged (as in the two $MM5_E$ and $MM5_S$ simulations). This has significant effects on the atmospheric conditions that lead to the onset of the precipitation. During this phase, the local conditions in the PBL, such as air humidity, temperature, and turbulence, that can be driven by the soil moisture conditions and evaporation process, can trigger or delay precipitation, especially in the flat terrain areas where there is no forcing due to the orographic lifting (center of domain 4). Once the precipitation starts and the soil moisture reaches saturation, the local conditions in the two simulations become similar, and the evolution of the precipitation is driven mainly by synoptic forcing, becoming predominant over the local conditions. For this reason, the differences in the precipitation amount and pattern become less evident between the two simulations as the event progresses.

4.2 Statistical analysis of the results

In order to have an objective methodology to evaluate and compare the ability of the two MM5 simulations to reproduce the observed rain structure and intensity, a statistical analysis of the results has been carried out. The goal was to be able to assess the impact of using ASAR soil moisture fields on the forecast by comparing the results of the simulations giving a broader allowance for errors in the predicted precipitation amounts. The results found for domain 4 are presented in this section.

The confusion matrix (or error matrix) between the measured values and the simulated values has been created for each of the MM5 simulations. The confusion matrix is used when dealing with more classes of measured and estimated precipitation values in a way similar to a contingency table (used when dealing with two rain/no rain classes). At each hour, eight classes of the measured 6 h accumulated precipitation (normalized to the maximum observed value found at each hour) have been created: the first class with a rainfall amount ranging between 0 and 20 % of the maximum amount observed, the second between 20 % and 30 % of the maximum amount observed, and so on, until the eighth class, with a rainfall amount larger than 80 % of the maximum observed.

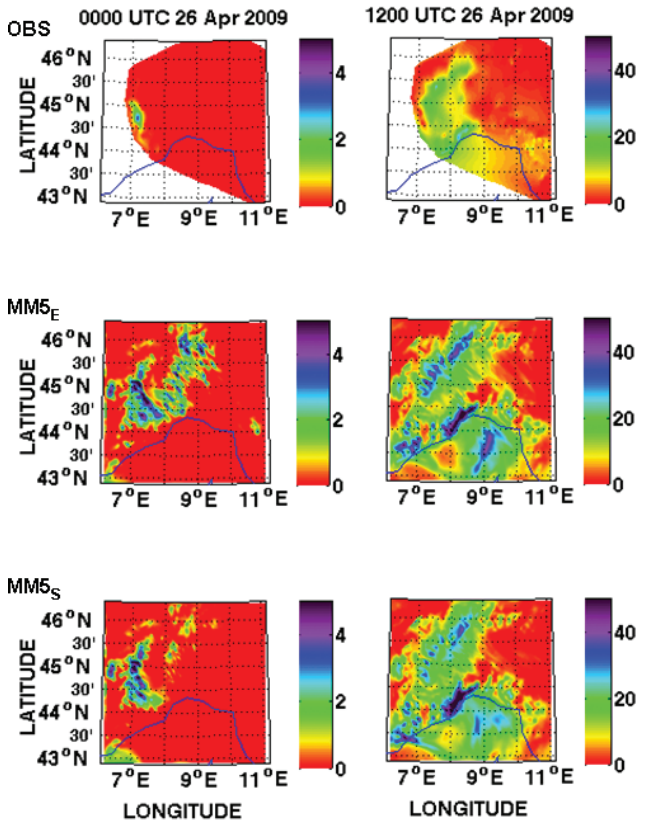

Fig. 8. 6 h accumulated precipitation (mm) on 26 April in domain 3 at 00:00 UTC (left panel) and 12:00 UTC (right panel).

The measured rainfall values (interpolated to the MM5 grid) have been associated to each of the eight rainfall classes, creating eight "TRUTH" classes. It is well-known that the sum of diagonal elements of the confusion matrix gives an estimate of the overall accuracy of the simulation, i.e. how well the observed rainfall intensity and location is reproduced by the model with respect to the observations. The confusion matrix was computed for both $MM5_E$ and $MM5_S$.

The left panel of Fig. 9 shows the overall accuracy of the two MM5 simulations (calculated as the sum of the diagonal elements of the confusion matrix divided by the total number of grid points) as a function of time (hours into the simulation after start time). The results are given only starting at the time when the observations show precipitation (after 26 April, 03:00 UTC, i.e. 27 h into the simulation). It is evident that the use of ASAR-retrieved SMC in the initial condition has a strong impact on the accuracy of the forecast at the early stage of the event by better predicting the location and the amount of the initial precipitation. As the simulation progresses, the accuracy is reduced, but the use of SMC from ASAR gives overall a better accuracy then the use of SMC from ECMWF analysis in the first 36 h, when the two forecasts are significantly different and the impact of the initial SMC condition is stronger. Then, the accuracy curves become similar, the forecast mostly determined by the large scale dynamics, and the soil saturated throughout domain 4 in both simulations.

In order to estimate the ability of the model to forecast precipitation amounts within the range of that observed, the percentage of grid points at each hour with accumulated precipitation larger than the maximum rainfall measured has been calculated. The right panel of Fig. 9 shows the evolution with time (hours since the start time) of the percentage of grid points with precipitation exceeding the highest precipitation amount registered by the rain gauges throughout domain 4. The data are shown only after the onset of precipitation on $MM5_E$; the $MM5_S$ performs significantly better than $MM5_E$. Before the 26th hour after start time (02:00 UTC, 26 April), when zero precipitation amounts are registered by the rain gauges, the curves represent the percentage of grid points where precipitation occurs. The $MM5_E$ shows that 20 % of the grid points have rain already at the 17th hour, and the percentage rises to 80 % at the 26th hour (02:00 UTC, 26 April). In the $MM5_S$, the rainy grid point percentage is much lower; it does not reach 20 % until 00:00 UTC, 26 April (24th hour) and it stays under 40 % at 02:00 UTC. After actual precipitation starts (the 27th hour, at 03:00 UTC, 26 April), the curves represent the ability of the model to predict rainfall amounts within the range of those observed. The use of SMC from ASAR reduces drastically the percentage of grid points where rainfall is overestimated until the 30th hour into the simulation, when the percentage is 15 % lower in $MM5_S$ than in $MM5_E$. The percentage in $MM5_S$ is as low as 3 % between the 27th and the 30th hours, and it increases linearly to about 20 % at the 36th hour, always significantly lower than $MM5_E$. After the 36th hour, the two curves become comparable and the tendency to overestimate the precipitation decreases in both simulations.

Three additional statistical parameters have been taken under consideration to evaluate the impact of SMC on the forecast: the misses, the hits, and the false alarms calculated on the rain/no-rain threshold (fixed at 0.2 mm) of the 6 h accumulated precipitation in the two simulations. The analysis was carried out only starting at the time when $MM5_E$ started producing rain. The upper left panel of Fig. 10 shows the evolution with time of false alarms, i.e. the fraction of grid points in domain 4 where the model predicts rain and the interpolated rain gauge data do not show precipitation. In $MM5_S$, the false alarms are dramatically reduced with respect to $MM5_E$, both before and after the time when the rain gauges start measuring non-zero precipitation. After the 30th hour into the simulation, the fraction of false alarms drops, meaning that both simulations are able to predict rain where it is observed. The upper right panel of Fig. 10 shows the hits of no-rain grid points, i.e. the number of grid points in domain 4 where both the rain gauges and the model do not show precipitation. Also, in this case $MM5_S$ predicts areas of no-rain better than $MM5_E$ before and after the onset of actual

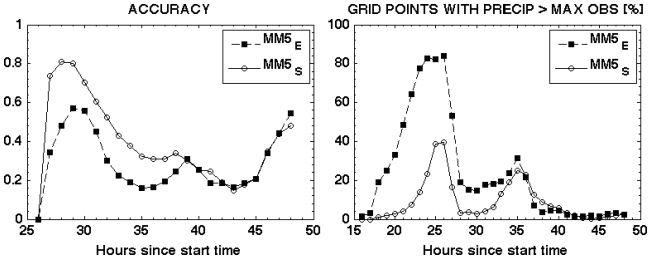

Fig. 9. Left panel: overall accuracy of MM5 in domain 4 as a function of time (hours into the simulation with start time at 00:00 UTC, 25 April). Right panel: percentage of grid points in domain 4 with 6 h accumulated precipitation higher than the maximum amount observed at each hour, for the $MM5_E$ and $MM5_S$ simulations, vs. time (hours since start time).

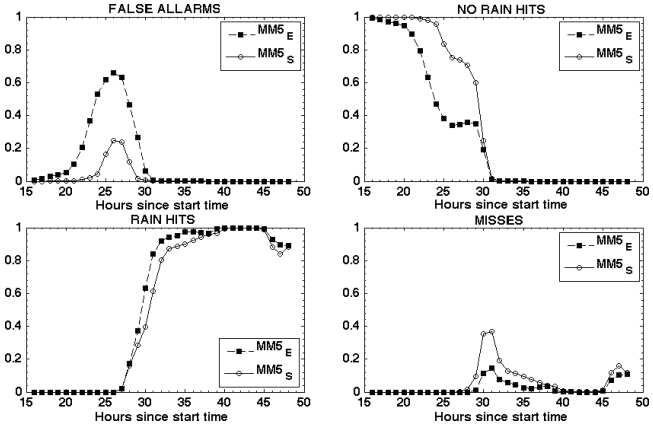

Fig. 10. Time evolution (hours since start time) of false alarms (upper left panel), hits of grid points where there is no rain (upper right panel), hits of rain (lower left panel) and misses (lower right panel), for the $MM5_E$ and $MM5_S$ simulations.

precipitation (26th hour, 02:00 UTC, 26 April). In the lower left panel, the hits of rain grid points are shown, i.e. the number of grid points where both the rain gauges and the model have precipitation. Here $MM5_E$ performs slightly better than $MM5_S$, meaning that some areas where the rain gauges give precipitation are missed by $MM5_S$. However, at the time of the onset of the precipitation (27th hour) the hits in the two simulations are almost identical. This result is confirmed in the lower right panel of Fig. 10, showing the misses, i.e. grid points where the observations show precipitation and the simulations do not show precipitation. The $MM5_S$ misses are larger than $MM5_E$ ones, especially at the 30th and 31st hour. At these times, the interpolated rain gauge data show very light precipitation in the center and in the northeast side of the domain, which is not correctly reproduced by $MM5_S$. This precipitation being very light represents a slight discrepancy with respect to rain gauge measurements that does not invalidate the general consideration on the improvement of the performances of the MM5 model when initialized with the SAR-derived moisture fields, demonstrated by the results expressed in terms of confusion matrix (i.e. overall accuracy). Moreover, the spread of light rain in the map of the interpolated rain gauge data might be an effect of the 2-D interpolation method itself used to for the sparse rain gauge stations in domain 4.

4.3 Interpretation of the results

In order to understand why the early phase of the event is so strongly influenced by the soil moisture, it is important to analyze how the soil evaporation process influences the PBL structure before the onset of the precipitation. Because of the night start time, there is no soil and/or canopy evaporation in the first hours of the simulations. It starts with the solar heating of the surface, at a rate that depends on the atmospheric conditions (temperature, humidity and wind) and the characteristics of the soil. Once the precipitation starts and wets the surface, the soil moisture reaches saturation and the soil moisture conditions in $MM5_S$ and in $MM5_E$ become the same, with the soil moisture approaching the field capacity. In $MM5_E$, the moisture flux into the PBL due to direct soil evaporation is higher than in $MM5_S$ solely because of the moister soil, all the other conditions remaining the same as in $MM5_S$ (vegetation parameters, soil parameters, atmospheric conditions). Before the precipitation starts, water vapour conditions in the PBL are significantly different in the two simulations, leading to a very different precipitation spatial distribution and intensity. This is shown in Fig. 11. These figures show the water vapour in the PBL in $MM5_S$ (left panels) and in $MM5_E$ (right panels) on a meridional cross section taken on the center of domain 4, on 25 April at 06:00 UTC (upper panels), before the soil evaporation is triggered by the incoming solar radiation, and at 22:00 UTC (lower panels), before the onset of the precipitation. In both simulations, $MM5_E$ and $MM5_S$, the soil moisture goes through a whole day with no precipitation during which the soil evaporation potentially takes place.

In the upper panels the water vapour mixing ratio cross sections for $MM5_S$ and $MM5_E$ look almost identical, while large differences can be found in the lower panels. As the simulation progresses, the effect of different initial soil moisture affects the water vapour distribution in the PBL, which, in turn, will affect the precipitation. This differentiation in the evaporation process, due to the different initial soil moisture, goes on until precipitation starts, and soil becomes saturated. In order to have a significant effect of soil moisture evaporation in the PBL structure and on the precipitation, there must be sufficient time for the soil moisture to be released into the atmosphere. In this case study, the change of PBL water vapor field due to the soil moisture evaporation starts after the first 7 h into the simulation, and the effect becomes more significant as the simulation proceeds. If the start time of the simulation is too close to the onset of the

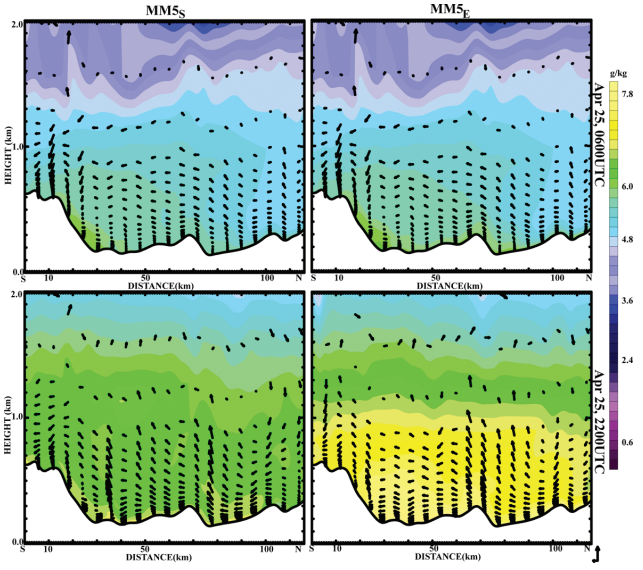

Fig. 11. North-South cross section of water vapour mixing ratio on 25 April at 06:00 UTC (upper panels) and 22:00 UTC (lower panels). Left panels: $MM5_S$ run; right panels: $MM5_E$ run.

precipitation, the impact of soil moisture is dramatically reduced. Moreover, if the start time is at night and the precipitation starts before sunrise, only very dry atmospheric conditions (or advection of very dry air) might trigger the soil evaporation process. In this case, being the event characterized by the flow of humid air at all levels, only the warming effect of the sun could create the conditions for soil direct evaporation and canopy evapo-transpiration to take place. This is also confirmed by the results of the simulations starting at 00:00 UTC of 26 April, where the water vapour field at the time of the onset of the precipitation (few hours after the start time) is not affected by the different soil moisture conditions.

5 Conclusions

In this study, the soil moisture retrieval from the ASAR C-band instrument on 24 April, at 20:53 UTC is used as the initial condition in the MM5 simulation of the Tanaro flood event in Northern Italy (26–28 April 2009) to evaluate the impact of high resolution soil moisture field on the precipitation forecast. Two MM5 simulations are carried out starting on 25 April, 00:00 UTC, for 48 h: one using the SMC available from the ECMWF analysis and one using the SMC field obtained by merging the high resolution data available from ASAR (available only for sparsely vegetated areas and bare soil) with ECMWF data. The precipitation produced by the model is compared to rain gauge data used as ground truth.

The merging procedure of the SMC data applied to the high resolution domain of the model, showed large differences between the mean values of the retrieved and the ECMWF data, with ECMWF showing much higher SMC values than ASAR. This "bias" is used to correct the ECMWF SMC in the outer domains. Moreover, the ASAR data showed high resolution features of dry and wet surface which reflected the highly variable land use in the Tanaro region, not represented in the ECMWF analysis.

The use of the ASAR-derived SMC to initialize the model shows a significant impact on the precipitation forecast, particularly evident during the early phase of the event. The timing of the onset of precipitation is significantly improved by delaying it towards the actual time registered by the rain gauges. The intensity of rainfall is lowered in most areas, more consistently with the observed amount of precipitation, and the rainfall overestimation areas are drastically reduced. Moreover, the no precipitation areas are better depicted and the percentage of false alarms drops significantly. In some cases, the areas with light precipitation are missed (but the light precipitation showed in the rain gauge data map might have been affected by an error in the 2-D interpolation of the rain gauge stations). The overall accuracy of the forecast using ASAR SMC data is significantly larger for the first 30 h of simulation.

The large impact of ASAR SMC on the precipitation has been mainly attributed to the different effect of soil evaporation in the PBL structure at the time prior to the onset of the precipitation. Large differences are found in the water vapour field for the two simulations ($MM5_E$ and $MM5_S$), because of the different impact of the SMC on the surface moisture fluxes. In both simulations the soil moisture goes through a whole day with no precipitation, during which soil evaporation takes place and affects the water vapour field in the PBL. All atmospheric and soil conditions being the same in both simulations except for the initial SMC, the differences could be attributed only to the drier soil conditions found from the ASAR retrievals with respect to the ECMWF analysis.

In order to have a significant effect of soil moisture evaporation in the PBL structure and on the precipitation, there must be sufficient time for the soil moisture to be released into the atmosphere. If the start time is during the night and the precipitation starts before sunrise, only very dry atmospheric conditions (or advection of very dry air) might trigger the soil evaporation process. In general, only the warming effect of the sun is likely to create the conditions for the soil direct evaporation and canopy evapo-transpiration to take place. According to the results of this study, it takes a few hours for the water vapour to be significantly affected by the soil evaporation processes. It is worth investigating further whether this delay in releasing surface moisture in the PBL is either due to the parameterization of the surface processes in the Land Surface Model or to the atmospheric conditions of this particular event or both.

This study represents a first attempt to establish whether high resolution SAR-based SMC data might be useful for operational use, in anticipation of the launch of the Sentinel-1 satellite. The response seems to be affirmative. However,

further investigations are needed in order to fully understand if the strong impact of SMC on the results seen in this study is related to the particular meteorological conditions of this event and to the specific model set-up used for this case. It will be essential to explore if there are specific meteorological conditions and characteristics of the NWP model used that would make the forecast more or less influenced by the use of high resolution SMC field as initial conditions. In general, in a wet soil, surface temperature does not change at the same rate as over a dry soil because solar energy is mostly used to evaporate water while it heats a dry surface, favouring local turbulence and forcing vertical velocities. However, the role of convection and local turbulence changes depending on the thermodynamic conditions (i.e. instability) and on the degree of synoptic forcing (i.e. convergence region of mesoscale circulation). Moreover, wind speed and air humidity play a crucial role in the effects of soil evaporation on the PBL. Based on the results of this study, we can anticipate that in the case of precipitation caused primarily by surface heterogeneity, the surface properties should be parameterized by proper resolution. In this case, the availability of high resolution soil moisture data from satellite such as ENVISAT/ASAR and Sentinel 1, might have a dramatic impact on precipitation forecast.

Acknowledgements. This work was supported by the Italian Space Agency (ASI) under the contract ASI No. I/036/07/0. The ECMWF is acknowledged for the data analysis. The NCAR is acknowledged for the MM5 model.

Edited by: A. Bartzokas
Reviewed by: A. M. Rossa and another anonymous referee

References

Alapaty, K., Niyogi, D., Chen, F., Pyle, P., Chandrasekar, A., and Seaman, N.: Development of the flux-adjusting surface data assimiation for mesoscale models, J. Appl. Meteor. Clim., 47, 2331–2350, 2008.

Attema, E. P. W. and Ulaby, F. T.: Vegetation modeled as a water cloud, Radio Sci., 13, 357–364, 1978.

Avissar, R. and Pielke, R.: A parameterization of heterogeneous land surfaces for atmospheric numerical models and its impact on regional meteorology, Mon. Weather Rev., 117, 2113–2136, 1989.

Ballard, S. P., Golding, B. W., and Smith, R. N.: Mesoscale model experimental forecasts of the Haar of northeast Scotland, Mon. Weather Rev., 119, 2107–2123, 1991.

Chen, F. and Avissar, R.: The impact of land-surface wetness on mesoscale heat fluxes, J. Appl. Meteor., 33, 1324–1340, 1994a.

Chen, F. and Avissar, R.: Impact of land-surface moisture variability on local shallow convective cumulus and precipitation in largescale models, J. Appl. Meteor., 33, 1382–1401, 1994b.

Chen, F. and Dudhia, J.: Coupling an advanced land surface-hydrology model with the Penn State-NCAR MM5 modeling system, Part I: Model implementation and sensitivity, Mon. Weather Rev., 129, 569–585, 2001.

Chen, F., Warner, T., and Manning, K.: Sensitivity of orographic moist convection to landscape variability: A Study of the Buffalo Creek, Colorado, flash-flood case of 1996, J. Atmos. Sci., 58, 3204–3223, 2001.

Chen, F., Manning, K. W., LeMone, M. A., Trier, S. B., Alfieri, J. G., Roberts, R., Tewari, M., Niyogi, D., Horst, T. W., Oncley, S. P., Basara, J. B., and Blanken, P. D.: Description and evaluation of the characteristics of the NCAR high-resolution land data assimilation system, J. Appl. Meteor. Climatol., 46, 694–713, 2007.

Comellas, A., Molini, L., Parodi, A., Sairouni, A., Llasat, M. C., and Siccardi, F.: Predictive ability of severe rainfall events over Catalonia for the year 2008, Nat. Hazards Earth Syst. Sci., 11, 1813–1827, doi:10.5194/nhess-11-1813-2011, 2011.

Dubois, P. C., van Zyl, J., and Engman, T.: Measuring Soil Moisture with Imaging Radars, IEEE Trans. Geosci. Remote Sens., 33, 915–926, 1995.

Dudhia, J.: A non hydrostatic version of the Penn State-NCAR mesoscale model: Validation tests and simulation of an Atlantic cyclone and cold front, Mon. Weather Rev., 121, 1493–1513, 1993.

Ferretti R., Low-Nam, S., and Rotunno, R.: Numerical simulations of the Piedmont flood of 4–6 November 1994, Tellus, 52, 162–180, 2000.

Ferretti, R., Paolucci, T., Graziani, G., Cherubini, T., Bernardini, L., and Visconti, G: Verification of high resolution real-time forecast over Alpine region during the MAP- SOP, Q. J. R. Meteorol. Soc., 129B, 587–607, 2003.

Grell, G. A., Dudhia, J. and Stauffer, D. R.: A description of the Fifth-Generation Penn State/NCAR Mesoscale Model (MM5), NCAR Technical Note NCAR/Tn- 398+STR. National Center for Atmospheric Research, PO Box 3000, Boulder CO80307-3000, USA, 1994.

Kain, J. S.: The Kain-Fritsch convective parameterization: an update, J. Appl. Meteor., 43, 170–181, 2002.

Mahfouf, J.-F., Viterbo, P., Douville, H., Beljaars, A., and Saarinen, S.: A Revised land-surface analysis scheme in the Integrated Forecasting System, ECMWF Newsletter, Summer-Autumn, 2000.

Mitchell, K. E., Lohmann, D., Houser, P. R., Wood, E. F., Schaake, J. C., Robock, A., Cosgrove, B. A., Sheffield, J., Duan, Q., Luo, L., Higgins, R. W., Pinker, R. T., Tarpley, J. D., Lettenmaier, D. P., Marshall, C. H., Entin, J. K., Pan, M., Shi, W., Koren, V., Meng, J., Ramsay, B. H., and Bailey, A. A.: The multi-institution North American Land Data Assimilation System (NLDAS): Utilizing multiple GCIP products and partners in a continental distributed hydrological modeling system, J. Geophys. Res., 109, D07S90, doi:10.1029/2003JD003823, 2004.

Oh, Y., Sarabandi, K., and Ulaby, F. T.: Semi-empirical model of the ensemble-averaged differentialMueller matrix for microwave backscattering from bare soil surfaces, IEEE Trans. Geosci. Remote Sens., 40, 1348–1355, 2002.

Pierdicca, N., Chini, M., Pulvirenti, L., and Macina, F.: Integrating Physical and Topographic Information into a fuzzy scheme to Map Flooded Area by SAR, Sensors, 8, 4151–4164, 2008a.

Pierdicca, N., Castracane, P., and Pulvirenti, L.: Inversion of Electromagnetic Models for Bare Soil Parameter Estimation from Multifrequency Polarimetric SAR Datadata, Sensors, 8, 8181–8200, 2008b.

Pierdicca, N., Pulvirenti, L., Bignami, C., Ticconi, F., and Laurenti, M.: High resolution mapping of soil moisture by SAR: data integration and exploitation of prior information, Proc. of IEEE/IGARSS 2009, Cape Town, South Africa, July 12–17, 2009.

Pierdicca, N., Pulvirenti, L., and Bignami, C.: Soil moisture estimation over vegetated terrains using multitemporal remote sensing data, Remote Sens. Environ., 114, 440–448, 2010.

Pleim J. E. and Gilliam, R.: An indirect data assimiation scheme for deep soil temperature in the Pleim-Xiu Land Surface Model, J. Appl. Meteor. Clim., 48, 1362–1376, 2009.

Pleim, J. E. and Xiu, A.: Development of a land surface model, Part II: Data assimilation, J. Appl. Meteor., 42, 1811–1822, 2003.

Polcher, J., McAvaney, B., Viterbo, P., Gaertner, M.-A., Hahmann, A., Mahfouf, J.-F., Noilhan, J., Phillips, T., Pitman, A., Schlosser, C. A., Schulz, J.-P., Timbal, B., Verseghy, D., and Xue Y. : A proposal for a general interface between land surface schemes and general circulation models, Glob. Planet. Change, 19, 261–276, 1998.

Pulvirenti, L., Chini, M., Pierdicca, N., Guerriero, L., and Ferrazzoli, P.: Flood monitoring using multi-temporal COSMOSkyMed data: image segmentation and signature interpretation, interpretation, Remote Sens. Environ., 115(4), 990–1002, 2011.

Rabin, R. M., Stadler, S., Wetzel, P. J., Stensrud, D. J., and Gregory, M.: Observed effects of landscape variability on convective clouds, B. Am. Meteorol. Soc., 71, 272–280, 1990.

Reisner, J., Rasmussen, R. M., and Bruintjes, R. T.: Explicit forecasting of supercooled liquid water in winter storms using the MM5 mesoscale model, Q. J. R. Meteorol. Soc., 124, 1071–1107, 1998.

Rotunno, R. and Ferretti, R.: Mechanisms of intense Alpine rainfall, J. Atmos. Sci., 58, 1732–1749, 2001.

Rotunno, R. and Ferretti, R.: Orographic analysis of rainfall in MAP cases IOP2B and IOP8, Q. J. R. Meteorol. Soc., 129B, 373–390, 2003.

Shafran, P. C., Seaman, N. L., and Gayno, G. A.: Evaluation of Numerical Predictions of Boundary Layer Structure during the Lake Michigan Ozone Study, J. Appl. Meteor., 39, 412–426, 2000.

Thompson, G., Rasmussen, R. M., and Manning, K.: Explicit forecasts of winter precipitation using an improved bulk microphysics scheme, Part I: Description and sensitivity analysis, Mon. Weather Rev., 132, 519–542, 2004.

Tramblay, Y., Bouvier, C., Martin C., Didon-Lescot, J. F., Todorovik, D., and Domergue, J. M.: Assessment of initial soil moisture conditions for event-based rainfall-runoff modelling, J. Hydrol., 387, 176–187, 2010.

Verhoest, N. E. C., Lievens, H., Wagner, W. Álvarez-Mozos J., Moran, S., and Mattia, F.: On the Soil Roughness Parameterization Problem in Soil Moisture Retrieval of Bare Surfaces from Synthetic Aperture Radar, Sensors, 8, 4213–4248, 2008.

Xiu, A. and Pleim, J. E.: Development of a land surface Model, Part I: Application in a mesoscale meteorological model, J. Appl. Meteor., 40, 192–209, 2001.